*universe*

MDPI

*Review*

# Stellar Microlensing Surveys as a Probe of Primordial Black Holes: Status and Prospects

**Anne M. Green**

School of Physics and Astronomy, University of Nottingham, University Park, Nottingham NG7 2RD, UK; anne.green@nottingham.ac.uk

**Abstract**

Stellar microlensing surveys are a powerful tool for probing dark matter in the form of planetary and stellar mass compact objects (COs) in particular primordial black holes (PBHs). Under standard assumptions, current observations exclude COs in the mass range $10^{-11} \lesssim M/M_\odot \lesssim 10^4$ making up all of the dark matter. We provide an overview, aimed at theorists working on PBHs, of the history, theory, observational status, and future prospects of the field.

**Keywords:** primordial black holes; microlensing; dark matter

## 1. Introduction and History

Stellar microlensing is the temporary magnification of a star which occurs when a compact object crosses the line of sight. It was first studied by Einstein, who concluded that 'there is no great chance of observing this phenomenon' [1]. However in 1986 Paczyński showed that by monitoring millions of stars in the Magellanic Clouds (MCs) it would be possible to probe compact objects (COs) in the Milky Way (MW) halo [2].

Various collaborations started microlensing surveys in the early 1990s, and the first MC candidate events were published in 1993 by EROS [3] and MACHO [4]. By the late 1990s the MACHO collaboration had observed significantly more events than expected from stars in the MCs or MW disk. This indicated that a significant fraction of the Milky Way halo could be in the form of roughly Solar mass COs [5,6]. Baryon budget arguments excluded such a large population of astrophysical objects (e.g., white dwarfs) [7]. Therefore it was suggested, e.g., Refs. [8,9], that these events could be due to primordial black holes (PBHs), black holes that may have formed in the early universe from large overdensities [10,11]. However the EROS [12–14] and OGLE [15,16] collaborations did not see a significant excess of events and instead constrained planetary and stellar mass COs to make up less than of order 10% of the MW halo.

In 2016 the discovery of gravitational waves from mergers of multi-Solar mass PBHs by LIGO-Virgo [17] generated a surge of interest in PBH dark matter (DM) [18–21]. However microlensing observations over two decades by the OGLE collaboration have failed to find the large, $\gtrsim 10^2$, number of events expected (under standard assumptions) if a significant fraction of the MW halo is in the form of stellar mass COs [22]. These long-duration observations have also increased the largest CO mass probed to $\sim 10^4 M_\odot$, while high-cadence observations by Niikura et al. have decreased the lowest mass to $\sim 10^{-11} M_\odot$ [23].

We overview how stellar microlensing surveys probe the fraction of COs, such as PBHs[1], in the MW halo by observing stars in the MCs or M31[2]. Our aim is to provide an

Check for updates

Academic Editors: Jeremy Mould and Lorenzo Iorio

Received: 19 February 2026
Revised: 13 April 2026
Accepted: 20 April 2026
Published: 25 April 2026

**Copyright:** © 2026 by the author. Licensee MDPI, Basel, Switzerland. This article is an open access article distributed under the terms and conditions of the Creative Commons Attribution (CC BY) license.

introduction to this field that is accessible to theorists who are interested in PBHs and specifically the possibility that planetary and stellar mass PBHs make up a significant fraction of the DM. First, in Section 2, we review the theory of stellar microlensing before focusing on observations in Section 3. We then look at future prospects in Section 4 before concluding with a brief summary in Section 5.

For an overview of the history of PBHs, see Ref. [27]. Refs. [28,29] review the formation of PBHs and the full range of observational probes of their abundance. For a review of the theory of microlensing see, e.g., Ref. [30], while Refs. [31,32] overview the observational status as of the 2010s.

## 2. Theory

In this section we overview the theory of stellar microlensing. First, in Section 2.1, we cover the basics of photometric microlensing, including individual events (Section 2.1.1) and the optical depth and event rate (Section 2.1.2). We then look at the differential event rate and parameter constraints (Section 2.2) and non-standard events (Section 2.3). Finally we conclude in Section 2.4 with a brief overview of astrometric microlensing.

### *2.1. Basics*

#### 2.1.1. Individual Events

In this subsection we overview the key properties of individual 'standard' photometric microlensing events where a point source is lensed by a point lens. For more details see, e.g., the original microlensing paper by Paczyński [2] or the review by Mao [30].

Microlensing occurs when the splitting of images caused by gravitational lensing is too small to be resolved, and instead the source is amplified by a factor [2,33]

$$A = \frac{u^2+2}{u\sqrt{u^2+4}}, \tag{1}$$

where $u = b/R_E$, $b$ is the distance of the lens from the line of sight to the source and $R_\mathrm{E}$ is the Einstein radius

$$R_\mathrm{E} = 2\left[\frac{GMD_\mathrm{L}(D_\mathrm{S}-D_\mathrm{L})}{c^2 D_\mathrm{S}}\right]^{1/2}, \tag{2}$$

where $G$ is the gravitational constant, $M$ is the mass of the CO, $D_\mathrm{S}$ is the distance from the observer to the source, and $D_\mathrm{L}$ is the distance to the lens. For a Large Magellanic Cloud (LMC) microlensing survey, $D_\mathrm{S} = 49.6\,\mathrm{kpc}$ [34] and

$$R_\mathrm{E} \sim 10^{-4}\,\mathrm{pc}\sqrt{x(1-x)}\left(\frac{M}{M_\odot}\right)^{1/2}\left(\frac{D_\mathrm{s}}{50\,\mathrm{kpc}}\right), \tag{3}$$

where $x = D_\mathrm{L}/D_\mathrm{S}$ is the fractional distance of the lens along the line of sight ($0 \leq x \leq 1$).

A microlensing event is usually determined to occur when $u \leq 1$, which corresponds to $A \geq A_\mathrm{T} = 1.34$. The timescale of the event, $\hat{t}$, is defined as the time taken to cross the Einstein diameter or radius. The EROS and OGLE collaborations use the Einstein radius crossing time, while the MACHO collaboration and this review use the Einstein diameter crossing time, $\hat{t} = 2R_\mathrm{E}/v_\mathrm{t}$, where $v_\mathrm{t}$ is the transverse speed of the lens relative to the line of sight. For lensing of stars in the LMC by the CO in the MW halo typically

$$\hat{t} \sim 1\,\mathrm{yr}\sqrt{x(1-x)}\left(\frac{M}{M_\odot}\right)^{1/2}\left(\frac{v_\mathrm{t}}{200\,\mathrm{km\,s^{-1}}}\right)^{-1}. \tag{4}$$

Due to the mass dependence of the timescale, observations over a long duration are needed to probe large masses, while high-cadence observations (i.e., at short intervals) are required to probe small masses.

Because the timescale, $\hat{t}$, depends on the lens mass, distance and velocity, it is not possible to measure the lens mass from the timescale of a single standard microlensing event (this is often referred to as the microlensing degeneracy). However, as we will see in Section 2.2, the lens mass can be probed statistically from the distribution of timescales, given a model for the lens density and velocity distributions. The Einstein crossing time, $\hat{t}$, is different from the time for which the amplification exceeds the threshold value $A_{\rm T} = 1.34$, $t_{\rm e}$, and has observational and theoretical advantages over $t_{\rm e}$[3]. Observationally, determining when the amplification crosses a particular threshold (and hence $t_{\rm e}$) is challenging, whereas $\hat{t}$ is found by fitting to the entire light curve. Theoretically, $t_{\rm e}$ depends on the impact parameter (as well as the lens mass, distance and velocity), which makes the calculation of the differential event rate more complicated.

The impact parameter relative to the Einstein radius, $u = b/R_{\rm E}$, can be written as

$$u = \left( \frac{2t^2}{\hat{t}^2} + u_{\rm min}^2 \right)^{1/2}, \tag{5}$$

where $u_{\rm min} = b_{\rm min}/R_{\rm E}$, $b_{\rm min}$ is the minimum value of the distance of the lens from the line of sight to the source, and time $t$ is defined so that $t = 0$ when $b = b_{\rm min}$. Figure 1 shows the geometry of a microlensing event, as viewed perpendicular to and along the line of sight, including $R_{\rm E}$, $D_{\rm S}$, $D_{\rm L}$, $b$ and $b_{\rm min}$. Figure 2 shows the magnification factor $A$, given by Equation (5), as a function of $2t/\hat{t}$ for different values of $u_{\rm min}$. This light curve, which is symmetric and achromatic (i.e., the same for all wavelengths), is often referred to as the Paczyński light curve.

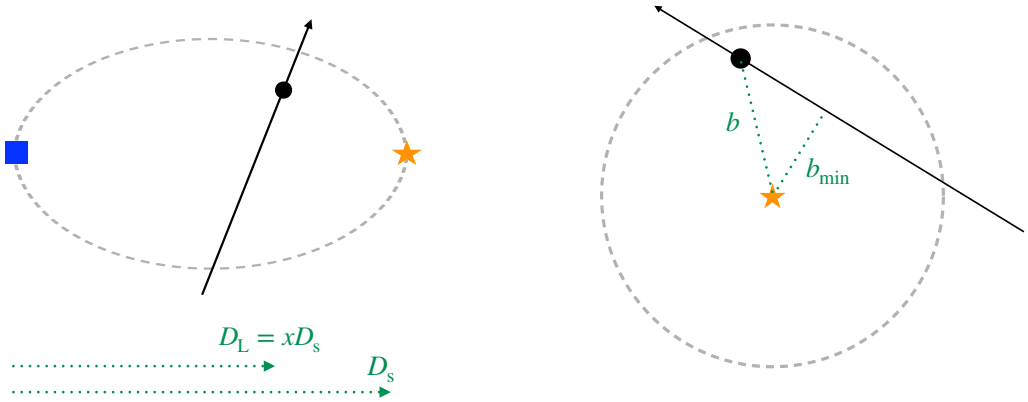



**Figure 1.** The geometry of a stellar microlensing event. The (**left**) and (**right**) panels show the view perpendicular to and along the line of sight respectively. The solid black and dashed grey lines show the trajectory of the compact object and the Einstein radius, $R_{\rm E}$, respectively. The orange star, black circle and blue square denote the source, the lens and the observer respectively. In the left panel the dotted green lines show the distance from the observer to the lens and source, $D_{\rm L} = xD_{\rm S}$ and $D_{\rm S}$ respectively. In the right panel the green dotted lines show the impact parameter, $b$, and its minimum value $b_{\rm min}$.

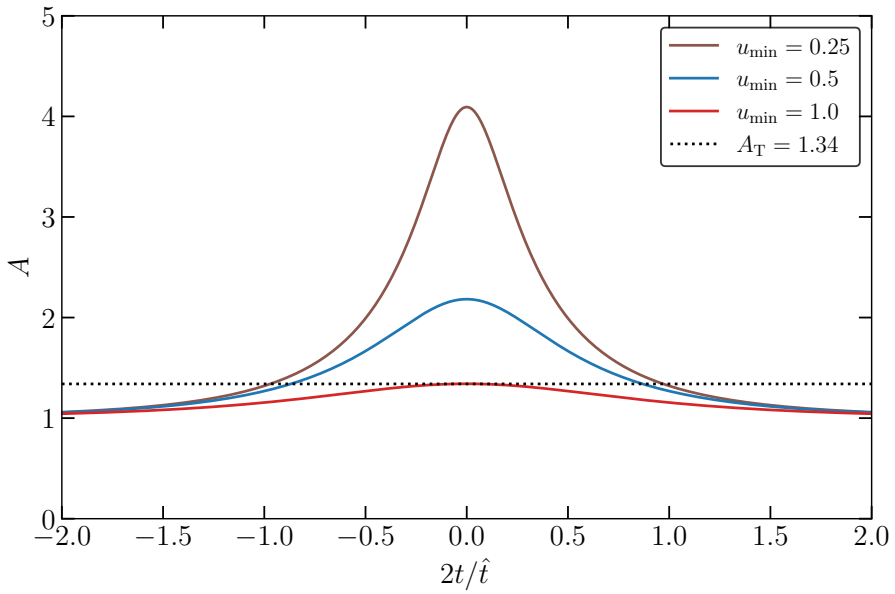



**Figure 2.** The magnification factor, $A$, Equation (5), as a function of $2t/\hat{t}$ for $u_{\rm min} = b_{\rm min}/R_{\rm E} = 0.25$, 0.5 and 1.0 (from top to bottom). The horizontal dotted black line shows the threshold for a microlensing event, $A_{\rm T} = 1.34$.

#### 2.1.2. Optical Depth and Event Rate

The optical depth, $\tau$, is the probability that a source star is being lensed at a given instant, i.e., that it falls within the Einstein radius of a lens:

$$\tau = \int_0^{D_{\rm S}} n(D_{\rm L}) \pi R_{\rm E}^2(D_{\rm L})\, {\rm d}D_{\rm L} = 4\pi G \int_0^{D_{\rm S}} \rho(D_{\rm L}) \frac{D_{\rm L}(D_{\rm S} - D_{\rm L})}{D_{\rm S}}\, {\rm d}D_{\rm L}\,, \tag{6}$$

where $n(D_{\rm L})$ and $\rho(D_{\rm L}) = n(D_{\rm L})/M$ are the number density and (mass) density of lenses respectively. Note that the dependence on the lens mass, $M$, of the number density and the square of the Einstein radius cancel, and hence the optical depth depends on the total mass density of lenses along the line of sight but not their individual masses. For a very simple model of the Milky Way (MW) halo with constant density and a circular speed $v_{\rm c} = \sqrt{GM(< D_{\rm S})/D_{\rm S}} \approx 220\,{\rm km\,s^{-1}}$, $\tau = v_{\rm c}^2/2c^2 \sim 10^{-6}$ [30]. This small optical depth means that to detect microlensing events it is necessary to monitor a large number, i.e., millions, of stars. Furthermore, it is extremely unlikely that a single star will undergo two independent microlensing events.

A more useful quantity is the rate, $\Gamma$, at which events occur, and we present a modified version of the illustrative calculation outlined in Ref. [30]. The area, ${\rm d}\tilde{A}$, swept out by a lens in a time interval, ${\rm d}t$, is given by the product of the diameter of the Einstein ring, $2R_{\rm E}$, and the distance travelled, $v_{\rm t}{\rm d}t$: ${\rm d}\tilde{A} = 2R_{\rm E}v_{\rm t}{\rm d}t = 4R_{\rm E}^2{\rm d}t/\hat{t}$. The probability, ${\rm d}\tau$, of an individual star undergoing a new microlensing event is given by

$${\rm d}\tau = n(D_{\rm L})\, \pi R_{\rm E}^2\, {\rm d}D_{\rm L}\,. \tag{7}$$

If $N_\star$ is the number of stars being monitored, then the number of new microlensing events in time ${\rm d}t$, ${\rm d}N$, is given by

$${\rm d}N = N_\star \int_0^{D_{\rm S}} n(D_{\rm d}) {\rm d}\tilde{A}\, {\rm d}D_{\rm d} = N_\star \int_0^{D_{\rm S}} n(D_{\rm d}) \frac{4R_{\rm E}^2}{\hat{t}}\, {\rm d}t\, {\rm d}D_{\rm d} = \frac{4N_\star}{\pi} \int_0^{D_{\rm S}} \frac{1}{\hat{t}} {\rm d}\tau\, {\rm d}t\,, \tag{8}$$

and hence the rate at which new events occur, $\Gamma$, is given by

$$\Gamma \equiv \frac{\mathrm{d}N}{\mathrm{d}t} = \frac{4N_\star}{\pi}\int_0^{D_\mathrm{S}} \frac{\mathrm{d}\tau}{\hat{t}}\,. \tag{9}$$

Assuming that all events have the same timescale $\hat{t}$ leads to a rough relationship between the event rate and optical depth:

$$\Gamma \sim \frac{4N_\star}{\pi\hat{t}}\tau\,. \tag{10}$$

### 2.2. Differential Event Rate and Parameter Constraints

Since the timescale of a microlensing event depends on the CO mass (as well as its position and velocity), the differential event rate, $\mathrm{d}\Gamma/\mathrm{d}\hat{t}$, i.e., the rate at which events of timescale $\hat{t}$ occur, can be used to probe the CO mass. The standard expression for the LMC differential event rate for a halo composed entirely of COs ($f = 1$, where $f$ is the fraction of the total mass of the halo in the CO) with mass $M$ and a smooth density distribution $\rho(r)$, is [5]

$$\frac{\mathrm{d}\Gamma_\mathrm{MW}}{\mathrm{d}\hat{t}} = \frac{32D_\mathrm{S}}{M\hat{t}^4 v_\mathrm{c}^2}\int_0^1 \rho(x)R_\mathrm{E}^4(x)\exp\left[-Q(x)\right]\mathrm{d}x\,, \tag{11}$$

where $Q(x) = 4R_\mathrm{E}^2(x)/(\hat{t}^2 v_\mathrm{c}^2)$. Note that Equation (11) assumes that the velocity distribution, $f(\mathbf{v})$, is Maxwellian

$$f(\mathbf{v})\,\mathrm{d}^3\mathbf{v} = \frac{1}{\pi^{3/2}v_\mathrm{c}^3}\exp\left(-\frac{v^2}{v_\mathrm{c}^2}\right)\mathrm{d}^3\mathbf{v}\,; \tag{12}$$

however, this is only true for an isotropic, isothermal sphere.

The standard halo model historically assumed in microlensing studies ('Model S' in, e.g., Ref. [5]) has a density profile

$$\rho(r) = \rho_0\,\frac{r_\mathrm{c}^2 + r_0^2}{r_\mathrm{c}^2 + r^2}\,, \tag{13}$$

and local dark matter density $\rho_0 \equiv \rho(r_0) = 0.0079 M_\odot \mathrm{pc}^{-3}$, core radius $r_\mathrm{c} = 5$ kpc, Solar radius $r_0 = 8.5$ kpc and circular speed $v_\mathrm{c} = 220\,\mathrm{km\,s}^{-1}$[4]. For the standard halo model, the differential event rate, Equation (11), becomes [5]

$$\frac{\mathrm{d}\Gamma_\mathrm{MW}}{\mathrm{d}\hat{t}} = \frac{512\rho_0(R_\mathrm{c}^2 + R_0^2)D_\mathrm{S}G^2M}{\hat{t}^4 {v_\mathrm{c}}^2 c^4}\int_0^1 \frac{x^2(1-x)^2}{A + Bx + x^2}\exp\left[-Q(x)\right]\mathrm{d}x\,, \tag{14}$$

where $A = (r_\mathrm{c}^2 + r_0^2)/D_\mathrm{S}^2$, $B = -2(r_0/D_\mathrm{S})\cos b\cos l$ and $b = -32.8^\circ$ and $l = 281^\circ$ are the Galactic latitude and longitude, respectively, of the LMC. Figure 3 shows the differential event rate for a standard halo composed entirely, $f = 1$, of COs with $M = 1M_\odot$. For different masses, the differential event rate scales as $M^{-1/2}$ and the timescales as $M^{1/2}$ [36]. For short-timescale events $\mathrm{d}\Gamma/\mathrm{d}\hat{t} \propto \hat{t}^2$, while for long-timescale events $\mathrm{d}\Gamma/\mathrm{d}\hat{t} \propto \hat{t}^{-4}$, independent of the CO distribution [37–39].

There are also contributions to the total differential event rate, $\mathrm{d}\Gamma/\mathrm{d}\hat{t}$, from stars ('$\star$') in the MW disc and LMC, and COs in the LMC:

$$\frac{\mathrm{d}\Gamma}{\mathrm{d}\hat{t}} = f\frac{\mathrm{d}\Gamma_\mathrm{MW}}{\mathrm{d}\hat{t}} + \frac{\mathrm{d}\Gamma_{\mathrm{MW},\star}}{\mathrm{d}\hat{t}} + \frac{\mathrm{d}\Gamma_{\mathrm{LMC},\star}}{\mathrm{d}\hat{t}} + f\frac{\mathrm{d}\Gamma_\mathrm{LMC}}{\mathrm{d}\hat{t}}\,. \tag{15}$$

Lensing by stars in the LMC, a possibility that was pointed out by Sahu [40], is often referred to as 'self-lensing'. The self-lensing rate is largest for observing fields in the centre of the LMC, where the number of stars is highest. The MACHO collaboration found, using models

of the LMC disc from Ref. [41], an optical depth $\tau_{\mathrm{LMC},\star} \sim (1-3) \times 10^{-8}$. Using the same LMC model with some minor modifications, OGLE III and IV (which has a wider observing field) found 5.7 events expected from stars in the LMC (compared with the $10^{2-3}$ expected if all of the halo is in planetary or stellar mass COs) [42]. The MACHO collaboration found an optical depth for microlensing by stars in the MW disc, $\tau_{\mathrm{MW},\star} \lesssim 10^{-8}$, lower than their estimate for self-lensing [6]. However more recent studies have found significantly larger MW disc rates, comparable with, or even larger, than the self-lensing rate, in part due to a larger thick disc contribution [42,43]. For the two MW models they considered [44,45], OGLE III and IV found 7.0 and 14.7 expected events respectively from stars in the MW disc [42]. Note, however, that the relative numbers of events from different lens populations depend on the fields observed and the detection efficiency (see below).

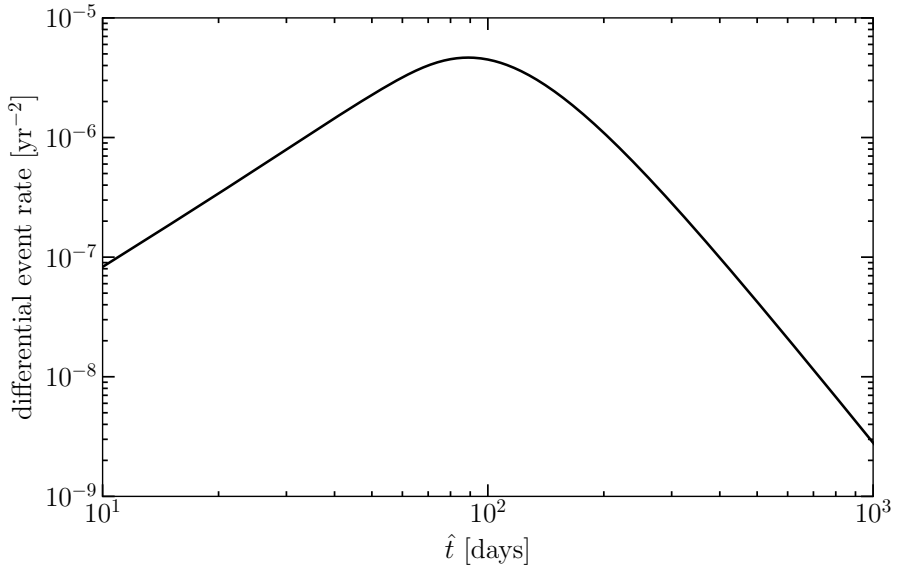



**Figure 3.** The differential event rate, $\mathrm{d}\Gamma/\mathrm{d}\hat{t}$, as a function of Einstein diameter crossing time, $\hat{t}$, for a standard halo (see text for details) composed entirely, $f = 1$, of COs with mass $M = 1M_{\odot}$ as given by Equation (14).

The total expected number of events, $N_{\mathrm{exp}}$, is given by

$$N_{\mathrm{exp}} = E \int_0^{\infty} \frac{\mathrm{d}\Gamma}{\mathrm{d}\hat{t}} \epsilon(\hat{t})\, \mathrm{d}\hat{t}\,, \tag{16}$$

where $E$ is the exposure (which is equal to the number of stars observed, $N_{\star}$, multiplied by the duration of the survey); $\epsilon(\hat{t})$ is the efficiency, i.e., the probability that a microlensing event with timescale $\hat{t}$ is detected (see Section 3.1); and $\mathrm{d}\Gamma/\mathrm{d}\hat{t}$ is the total differential event rate given by Equation (15). If no events are detected, then the 95% confidence limit on the fraction of the MW halo in COs can be calculated as $f = 3.0/N_{\mathrm{exp}}(f=1)$, where $N_{\mathrm{exp}}(f=1)$ is the expected number of events if $f = 1$. Surveys with a large exposure expect to observe events due to stars in the MW disc and/or LMC, and in this case constraints on the CO mass and halo fraction are calculated using the likelihood [6,42]

$$\mathcal{L}(f, M) = \exp\left(-N_{\mathrm{exp}}\right) E \prod_{i=1}^{N_{\mathrm{obs}}} \frac{\mathrm{d}\Gamma}{\mathrm{d}\hat{t}}(\hat{t}_i)\epsilon(\hat{t}_i)\,, \tag{17}$$

where $N_{\mathrm{obs}}$ is the number of observed events and $\hat{t}_i$ are their timescales. PBHs are expected to have an extended mass function (see, e.g., Section 2 of Ref. [29]). Constraints calculated assuming all COs have the same mass can be translated into constraints for a specific

extended mass function using the method presented in Ref. [46]. Furthermore, as pointed out in Ref. [37], if $f = 1$ is excluded for a particular range of masses under the assumption that all COs have the same mass, then any extended mass function with $f = 1$ in this range is excluded. We note that the constraints apply to any COs in the MW halo; however (as mentioned in the introduction), astrophysical objects, such as white dwarfs, are excluded from making up a large fraction of the halo by baryon budget arguments [7]. Ref. [47] has recalculated the microlensing constraints for extended objects, such as boson stars.

The MACHO first year results paper [5] studied a very wide range of models for the MW halo, some of which are not consistent with current observations. They found that there was a significant variation in the differential event rate and hence the observational constraints on the CO mass and halo fraction. The OGLE collaboration finds that the uncertainty in their constraint is relatively small (see Extended Data Figure 1 of Ref. [22]); however, they only consider two benchmark models (with fixed parameter values) and assume a Maxwellian velocity distribution. Other studies [48–51] have found that the uncertainty in exclusion limits can be significant. Ref. [52] found that the rate of long-timescale events (and hence the constraints on low-mass COs) has a fairly weak dependence on the CO density and velocity distribution. However the rate of short-timescale events (and hence the constraints on high-mass COs) depends sensitively on the local DM velocity distribution. An accurate calculation of the uncertainties on the differential event rate (and parameter constraints) for models consistent with current observations, and numerical simulations of Milky Way-like galaxies, is an outstanding issue.

Microlensing observations towards the Small Magellanic Cloud (SMC) could in principle help discriminate halo-lensing from self-lensing as the visible components of the SMC are elongated along the line of sight. The self-lensing rate is therefore expected to be larger than for the LMC. Furthermore for halo lenses, the timescales of events towards the LMC and SMC should be similar whereas for self-lensing, events towards the SMC are expected to be longer (due to the larger lens–source separation and hence Einstein radius) [53]. There are, however, significant uncertainties in the SMC's structure due to its tidal interactions with the LMC. See Refs. [54,55] for discussion of the status as of the late 1990s in the context of microlensing and, e.g., the Introduction of Ref. [56] for the current status in a more general context.

Microlensing surveys towards the Galactic bulge can be used to probe CO DM (see Sections 3.4 and 4.1). However in this case it is necessary to distinguish events due to CO DM in the MW halo from the large population of events caused by astrophysical objects in the luminous components of the MW.

Crotts explored the advantages and disadvantages of microlensing observations towards M31 (our nearest neighbour galaxy, also known as Andromeda) [57]. In particular he pointed out that the high inclination of M31's disc with respect to the line of sight would lead to a large asymmetry in the microlensing rate from lenses in the halo of M31. The event rate for the far side of the disc would be much higher than that for the near side due to the larger column density of halo lenses. This would be a potentially powerful tool for discriminating events due to halo lenses from self-lensing or variable stars. Baillon et al. [58] pointed out that the large number of source stars is another advantage of M31 over the MCs. However individual stars are not resolved, and hence 'pixel' lensing techniques are required (see Section 3.4). See Refs. [59,60] for theoretical studies of microlensing towards M31, including calculations of the differential event rate.

The standard calculation of the halo differential event rate outlined above, Equation (11), assumes that the CO dark matter distribution is smooth and fully specified by the density profile, $\rho(r)$. However PBH dark matter is expected to cluster more on sub-Galactic scales than particle dark matter. Since PBHs are discrete objects, there are Poisson fluctua-

tions in their distribution, and PBH clusters start forming shortly after matter–radiation equality [61,62]. For PBHs formed from Gaussian fluctuations, the clusters are sufficiently diffuse [63] that the PBHs still act as individual microlenses. In this case the effect on the microlensing differential event rate and hence constraints on the PBH mass and halo fraction are small [64,65]. Some PBHs are expected to be in binaries, which could potentially lead to a source being lensed twice; however, the binaries are typically sufficiently wide that the time between such repeating events is expected to be much longer that the duration of microlensing surveys [64]. The probability distribution of perturbations that are large enough to produce PBHs, which make up a significant fraction of the dark matter, is expected to be non-Gaussian, e.g., Ref. [66], however, and PBHs formed from non-Gaussian fluctuations can form more compact clusters [67]. If clusters are sufficiently compact that the cluster as a whole acts as a microlens, then microlensing parameter constraints (or allowed regions) will shift to lower PBH masses [50].

### *2.3. Non-Standard Events*

Deviations from the 'single point source, single point lens' assumptions underlying the standard Paczyński light curve, Equation (1), can have observable consequences. For a more detailed review see Ref. [30]. We discuss specific observed non-standard events in Section 3.2.

The standard light curve is significantly modified if the impact parameter of an event is comparable to the ratio of the radius of the source star to the Einstein radius [68,69]. In particular *finite source* effects significantly reduce the maximum magnification for COs with mass $M \lesssim 10^{-9} M_\odot$ [70].

The standard analysis assumes all motions are linear. However this is not the case if the lens or source are binary, and the Earth's orbit about the Sun also violates this assumption [71]. The *parallax* effect, due to the Earth's orbit, is detectable if the event timescale is not significantly shorter than a year [71]. For a *binary source*, orbital motion leads to periodic distortions in the light curve [72]. This is commonly referred to as the 'xallarap' effect (the inverse of parallax). A *binary lens* can generate complex, multi-peaked light curves with caustics (where the magnification formally diverges) [73].

PBHs with mass $M_{\rm PBH} \lesssim 10^{-11} M_\odot$ have Schwarzschild radius comparable to the wavelength of light, resulting in diffraction and interference effects. These *wave optics* effects reduce the magnification and place a lower limit on the mass of PBHs that can be probed by microlensing [74,75].

Some of these effects can break the microlensing degeneracy mentioned above, and allow the lens mass and/or projected transverse velocity to be measured. The latter is useful as it acts as a diagnostic for the lens location [76]. For lenses in the MW halo and LMC, the projected transverse velocity is determined by the velocity dispersion of the MW halo and LMC, which are small and large respectively. For lenses in the MW disc it is determined by the differential rotation of the Sun and disk, which has an intermediate value.

### *2.4. Astrometric Microlensing*

The above discussion focuses on photometric microlensing, i.e., the change in the apparent brightness of a source during a microlensing event. This is the observable used by the microlensing surveys to date, which we will overview in Section 3. Astrometric microlensing is the change in the apparent position of the source [77,78], and in the future telescopes which accurately measure the positions of stars (astrometry) will also be able to probe CO DM using astrometric microlensing (see Section 4.1).

The centroid shift of the source, $\delta\theta(u)$, is given by

$$\delta\theta(u) = \frac{u}{u^2+2}\theta_{\rm E}\,, \tag{18}$$

where $\theta_{\rm E}$ is the angular Einstein radius, $\theta_{\rm E} = R_{\rm E}/D_{\rm L}$. Using Equation (2), $\theta_{\rm E}$ can be expressed in terms of the lens–source parallax, $\pi_{\rm rel}$,

$$\frac{\pi_{\rm rel}}{\rm mas} = \frac{\pi_{\rm L}}{\rm mas} - \frac{\pi_{\rm S}}{\rm mas} = \frac{\rm kpc}{D_{\rm L}} - \frac{\rm kpc}{D_{\rm S}}\,, \tag{19}$$

in milliarc (mas), as

$$\theta_{\rm E}^2 = 8.144\,{\rm mas}\left(\frac{M}{M_\odot}\right)\pi_{\rm rel}\,. \tag{20}$$

Therefore if the parallax can also be measured, the lens mass can be determined [77,79]. Astrometric microlensing signals are detectable for large lens–source separations, so the optical depth is larger than for photometric microlensing [80,81].

## 3. Observations

In this section we first overview the general principles of stellar microlensing observations (Section 3.1) before looking at the results of specific surveys which have published constraints on the halo fraction of COs in Sections 3.2–3.6. Unless otherwise mentioned, all limits (or parameter values) quoted assume that the MW halo is described by the standard halo model (see Section 2.2) and that all COs have the same mass. Section 3.7 contains a summary of the current observational status. Figure 4 shows the final published parameter constraints on the halo fraction, $f$, and CO mass, $M$. Table 2 summarizes the main features of the key LMC microlensing surveys, including the number of events they observed. This section aims to provide theorists with an introduction to the general principles and current status of microlensing surveys. For further details see Ref. [31], a 2010 review of microlensing from an observational perspective.

### *3.1. General Principles*

The first step in analysing data from a microlensing survey is to generate light curves for individual objects. Historically this was done using point spread function photometry, e.g., Refs. [12,82]. More recently, different image analysis (DIA), which is more computationally demanding but better suited to the crowded stellar fields in the MCs, has been used, e.g., Refs. [13,83].

Candidate microlensing events are selected by applying a series of cuts to the light curves. These cuts are designed to select light curves which are well fit by the standard Paczyński form with a single, achromatic, symmetric variation as described in Section 2.1.1 while rejecting backgrounds that can mimic microlensing. Key backgrounds are supernovae in background galaxies and variable stars [6]. A class of variable star that has recurrent bumps in their light curve that mimic microlensing, so-called 'blue bumpers', were in fact discovered by microlensing surveys [37]. The detection efficiency, $\epsilon(\hat{t})$, is estimated by ascertaining what fraction of simulated events pass the selection cuts, e.g., Ref. [82]. The detection efficiency is necessarily zero for timescales shorter than the interval between observations (i.e., the cadence of the survey). Typically it grows with increasing timescale to a maximum value of order 40%, before declining to zero again for timescales longer than the duration of the survey [6,14,84].

As discussed in Ref. [85], selection criteria inevitably have to balance false positives (candidate events that are not due to microlensing) and false negatives (microlensing events that are rejected). The detection efficiency calculation takes into account the later but not the

former. Event selection (and detection efficiency estimation) is complicated by the ∼10% of microlensing events, which are 'exotic' and do not follow the standard Paczyński light curve produce by a single point source and lens, e.g., Ref. [86]. In some cases, e.g., MACHO-LMC-9, which we discuss further in Section 3.2, the event is unambiguously microlensing, and the features in the light curve provide information about the location of the lens. However in other cases non-microlensing variability can be fit by a non-standard lens model (see discussion in Ref. [86]). As discussed further in Section 3.2, in their final 5.7 year results, the MACHO collaboration used two sets of selection criteria: A, designed to detect high-quality simple events, and B, designed to also select exotic and lower signal to noise events [6]. EROS-2 [14] and OGLE [84] carried out manual inspections of a subset of their light curves to check for a significant population of overlooked events.

The measured optical depth can be estimated using

$$\tau = \frac{1}{E}\frac{\pi}{4}\sum_i \frac{\hat{t}_i}{\epsilon(\hat{t}_i)}\,, \tag{21}$$

where $\hat{t}_i$ is the estimated timescale of the $i$-th event. The estimated timescales and detection efficiency can also be used in a likelihood analysis, using Equation (17), to probe the CO mass and halo fraction. Note that what appears to be a single star in a survey can in fact be composed of several, unresolved, stars, a phenomenon known as blending. This affects the determination of the optical depth and event rate in multiple ways. It affects the estimation of the timescales of blended events, $\hat{t}$, and the detection efficiency, $\epsilon(\hat{t})$ [87]. It also means the effective number of stars monitored, $N_\star$, is larger than the number of catalogued objects. The impact of blending can be minimized, as is done by the EROS and OGLE collaborations, by only using bright red giant stars. See Ref. [31] for a more detailed overview.

### *3.2. MACHO*

Between 1992 and 1999 the MACHO collaboration monitored over 10 million stars in the LMC. Their first year results contained 3 candidate events, and (assuming all 3 were due to lens in the MW halo) they found a best-fit halo fraction $f = 0.2^{+0.2}_{-0.1}$ and a MACHO mass $M = 0.065^{+0.06}_{-0.03} M_\odot$ [37]. In their 2-year data they found 8 candidate events [5]. MACHO-LMC-2 and 3 from their 1-year data set did not pass the revised event selection cuts used in the 2-year analysis (and one of these two events subsequently brightened again repeatedly and is therefore thought to be a variable star). On the other hand, 3 of the 8 2-year-candidates were in the 1-year data but did not pass the 1-year cuts [5]. MACHO-LMC-9 had a U-shaped light curve, characteristic of a binary lens and, if the source star is single, the lens is likely to lie in the LMC [88]. Using a sub-sample of 6 events (excluding the binary lens, MACHO-LMC-9, and MACHO-LMC-10, which they deemed a marginal candidate) they found a halo fraction $f = 0.5^{+0.3}_{-0.2}$ and a MACHO mass $M = 0.5^{+0.3}_{-0.2} M_\odot$. A specific search for short timescale events in the 2-year data excluded COs in the range $3 \times 10^{-7} \lesssim M/M_\odot \lesssim 5 \times 10^{-4}$ making up all of the MW halo [89]. A subsequent EROS-MACHO joint analysis tightened this limit to $f < 0.10$ for this planetary mass range [90].

The final MACHO results were based on 5.7 years of observations [6]. They used two sets of selection criteria. Criteria A used similar cuts to their two year analysis [5] and were designed to select simple microlensing events, with a single, high significance bump in the light curve and a flat baseline. Criteria B were intentionally looser (with higher detection efficiency) and designed to search for exotic and/or low signal-to-noise events. Marginal events suspected of being supernovae in background galaxies were included in set B but rejected from set A. Set A contained 13 events (MACHO-LMC 1, 4, 5, 6, 7, 8, 13, 14, 15, 18, 21, 23 and 25), while an additional 4 events (9, 20, 22 and 27) passed criteria B[5]. The best-fit halo fraction (assuming a standard halo) decreased to $f \approx 0.2 \pm 0.1$, with the best-fit

mass remaining of order $0.5M_{\odot}$. The contribution of the MW disk and LMC to the total differential event rate was taken into account, with ∼3 events expected to be due to stars.

Follow-up observations have subsequently revealed further information about the nature of the lenses in some events. We summarize these developments; see also Ref. [91] for more extensive recent discussion. Ref. [86] presented additional data for MACHO-LMC-4, 13 and 15. They found that all 3 events were well fit by a standard Paczyński light curve, supporting their microlensing interpretation. Ref. [86] also discussed the interpretation of other MACHO events. The light curve of MACHO-LMC-23 deviated from the standard Paczyński form, and EROS and OGLE both observed the star brightening again [14,86,92], so it is therefore very unlikely to be a microlensing event.

MACHO-LMC-5 is a so-called 'jerk-parallax' event [93], where the light curve depends on the 2nd derivative of the Earth's velocity [94]. Analysis of Hubble Space Telescope data allowed the parallax and proper motion of the lens to be measured and the lens identified as an M dwarf star in the MW disk [93], as suggested by Ref. [95]. High-resolution follow-up data from the Global Microlensing Alert Network found a periodic modulation in the light curve of MACHO-LMC-14 [96]. These oscillations are thought to be the so-called 'xallarap' effect, which occurs when the source is binary [72]. This allowed the lens projected velocity to be estimated, and the resulting value is more consistent with expectations for a lens located in the LMC than the MW [96]. The light curve of MACHO-LMC-1 has an anomaly near its peak, which suggests that the lens is binary [91,97,98].

Follow-up infrared observations of MACHO-LMC-20 (which passed the B criteria) identified the lens as a M dwarf in the MW disk [99]. Follow-up observations of MACHO-LMC-22 (which was excluded from set A by hand) found that the source is extended and has emission lines not characteristic of stars and is therefore now thought to be a supernova or active Galactic nucleus in a background galaxy [100]. After MACHO-LMC-22 is excluded, none of the MACHO LMC events have Einstein diameter crossing times longer than 150 days, which excludes the CO with mass $0.3 \lesssim M/M_{\odot} \lesssim 30$ making up more than ∼60% of the MW halo [100].

Belokurov, Evans and Le Du analysed the MACHO light curves using neutral networks and concluded that 7 of the criteria A events (MACHO-LMC-1, 5, 6, 14, 23[6] and 25) were convincing microlensing candidates [101]. Bennett also revisited the interpretation of the 13 set A MACHO events [102]. He found that 7 of the events are confirmed microlensing candidates (MACHO-LMC-1, 4, 5, 13, 14, 15 and 25) and argued that between 10 and 12 events are likely to be microlensing (with the up to 2 remaining events being variable stars), significantly larger than the ∼2–3 events expected from stars in the MW or LMC, and consistent with $f \approx 0.16 \pm 0.06$ of a standard MW halo being in the CO. Subsequently, OGLE found that MACHO-LMC-7 (which was labelled 'unconfirmed' by Bennett [102]) varied repeatedly and is hence a variable star [92]. OGLE also found that MACHO-LMC 8 and 18 (which were also labelled 'unconfirmed' in Ref. [102]) had periodic variability in their baseline [22]. They argue that this is not common for microlensing events, and hence these events are likely due to variable stars, and the best-fit halo fraction is in fact ∼40% smaller than the value ($f \approx 0.2$) originally found in Ref. [6]. Two of the MACHO set A events occurred during the operation of EROS-2 [14]. The star in MACHO-LMC-15 was too dim to be seen by EROS-2, while MACHO-LMC-14 was observed by EROS2 but only in one colour and was therefore not included in their sample.

As part of their response to criticism by Hawkins and García-Bellido [103], the OGLE collaboration have published a reanalysis of the MACHO candidate events using more modern DIA techniques [91]. They deem events MACHO-LMC-6, 13 and 15 weak candidates due to their light curves being either asymmetric or lacking sufficient data around the peak. They note, however, that Bennett et al. [86] presented additional follow-up

photometry which supported the microlensing interpretation of events 13 and 15. Based on their new DIA light curves, they conclude that 7 of the MACHO events are very likely microlensing (MACHO-LMC-1, 4, 5, 9, 14, 21, 25) and argue that the other candidate events would be unlikely to pass 'sensible microlensing cuts'.

Table 1 contains a summary of the current status of the 13 events which passed criteria A. Of the 13 events, 4 are now thought to be variable stars and 2 are microlensing events with the lens likely not in the MW halo. This leaves at most 7 candidate lensing events where the lens could be located in the MW halo.

The MACHO collaboration did not publish CO constraints from observations towards the SMC, but they did observe 2 candidate microlensing events: MACHO97-SMC-1 [104] (which was also detected by EROS [54] and OGLE [105]) and MACHO98-SMC-1. The later was a caustic crossing binary lens event. Its live detection facilitated observations by multiple microlensing collaborations and an accurate measurement of a low value for the lens projected motion, indicating that the lens is likely in the SMC than the MW halo [106].

**Table 1.** A summary of the current status of the 13 events which passed criteria A in the 5.7 year MACHO collaboration analysis [6] (see also Table 1 of Ref. [91]). The 2nd column ('Microlensing') contains information on whether the event is currently thought to be microlensing. Events classified as 'very likely microlensing' and 'weak candidate' by Ref. [91] are denoted by a green tick, ✓, and an orange question mark, ?, respectively. Candidate events that are now thought to be variable stars are denoted by a red cross, ✗. The 3rd column ('Lens') contains information about the lens. It is left blank where there is no information and contains 'n/a' for events which are now thought to be variable stars.

| Event | Microlensing | Lens |
|---|---|---|
| 1 | ✓ | possibly binary [91,97,98] |
| 4 | ✓ | |
| 5 | ✓ | star in MW disk [93] |
| 6 | ? | |
| 7 | ✗ variable star (has varied repeatedly) [92] | n/a |
| 8 | ✗ likely a variable star [22] | n/a |
| 13 | ? | |
| 14 | ✓ | likely in LMC [96] |
| 15 | ? | |
| 18 | ✗ likely a variable star [22] | n/a |
| 21 | ✓ | |
| 23 | ✗ brightened a 2nd time, likely a variable star [86] | n/a |
| 25 | ✓ | |

### *3.3. EROS*

EROS ran from 1990 to 2003. Its first phase, EROS-1, found two candidate LMC events [12,107]. These events were compatible with microlensing by COs with mass $\approx 0.1 M_\odot$. However, because of the unusual nature of these events (the source star for one was an eclipsing binary star [12]), and the possibility of having detected variable stars, they chose to place an upper limits on the halo fraction: $f < 0.2$ for $10^{-7} \lesssim M/M_\odot \lesssim 0.01$. A dedicated search for short-timescale events excluded planetary mass COs, with mass $10^{-7} \lesssim M/M_\odot \lesssim 10^{-4}$, making up more than 10% of the MW halo [108].

In their first two years of SMC observations, EROS-2 found one candidate event, EROS2-SMC-1 [54,109], also detected by MACHO (MACHO97-SMC-1) [104] and OGLE [105]. In the first 2 years of EROS-2 LMC observations they found 2 events (EROS2-LMC-3 and 4). Combined with their surviving previous candidate events (EROS-LMC-2 was eliminated having undergone a 2nd variation [13]) they excluded COs with $10^{-7}(10^{-6}) \lesssim M/M_\odot \lesssim 1(10^{-3})$ making up more than 40(10)% of the MW halo [13].

With three more years of SMC observations EROS-2 found an additional three events (EROS2-SMC-2-4), with Einstein radius crossing times $> 200$ days (longer than the events observed towards the LMC) [110]. They argued that these events 'seem more compatible with unidentified variable stars or self-lensing within the cloud than with halo objects'. This was partly based on a prior expectation that halo COs would not have super-Solar masses; however, follow-up observations concluded that these events were indeed long-period variables [14]. The SMC observations placed slightly weaker constraints on the halo fraction than the previous LMC observations.

The final EROS-2 analysis used observations of a subsample of 7 million bright stars in the MCs, in order to aid discrimination of variable stars and minimize the effects of blending [14]. They found only one event, and constrained COs with $10^{-6} \lesssim M/M_\odot \lesssim 1$ to make up less than 10% of the MW halo. Section 6 and Table 4 of Ref. [14] contains an update on the status of the 11 previously published EROS MC events. Only 1 (EROS-SMC-1) remains a microlensing candidate. EROS1-LMC-1 and 2, and EROS2-LMC-3 and 4 underwent a 2nd variation. With improved data analysis EROS2-LMC-5, 6 and 7 were classified as supernovae, and (as mentioned above) additional data showed that EROS2-SMC-2, 3 and 4 were long-period variable stars.

Ref. [111] combined archival data from EROS-2 and MACHO to probe long timescale events and concluded that COs with mass $10 \lesssim M/M_\odot \lesssim 100(10^3)$ have $f < 0.15(0.5)$. Combined with the previous EROS results, $f > 0.15$ was excluded for $10^{-6} \lesssim M/M_\odot \lesssim 100$.

### *3.4. OGLE*

The OGLE project has run for more than thirty years, starting in 1992 [112]. The first OGLE MC observations (OGLE-II) found two candidate LMC events [15]. They found that if both were due to COs the halo fraction was $f = 0.08 \pm 0.06$. However they argued that these events were consistent with expectations from self-lensing and constrained the CO with $0.01 \lesssim M/M_\odot \lesssim 0.2$ to make up less than 10% of the MW halo. OGLE-LMC-02 subsequently underwent multiple additional brightenings and is therefore not a microlensing event [22]. Their initial observations towards the SMC found a single, unconvincing, candidate and slightly weaker limits [113].

In 8 years of observations towards the SMC, OGLE-III found 3 convincing events (OGLE-SMC-2-4) [16]. The light curve of OGLE-SMC-2 exhibits a clear parallax effect and also deviates from the simple Paczyński curve around its peak. Follow-up observations (including data from the Spitzer space telescope) measured the lens projected velocity and found that the lens is most likely a BH binary in the MW halo, with mass $M \sim 10 M_\odot$ [114]. Ref. [16] argued that this event is consistent with BHs making up of order a percent of the MW halo. Like MACHO-LMC-5, OGLE-SMC-3 was a jerk-parallax event, with the lens likely a M dwarf in the MW disc [16]. The combined OGLE-II and III MC limits on the halo fraction were similar to those from EROS2 for $M \gtrsim 0.01 M_\odot$ [16].

Results from OGLE-III and IV observations of 78.7 million stars in the LMC for up to 20 years were published in 2024 [22]. Their automated data pipeline found 13 events, all with Einstein radius crossing times less than one year. A manual, 'by eye', search found an additional 3 events. They found that the number of events, and their positions, timescales and parallaxes, are consistent with expectations from stars in the MW disk and the LMC. Using the 13 events identified using the automated data pipeline, they found that COs in the mass range $10^{-4}(10^{-5}) \lesssim M/M_\odot \lesssim 6(900)$ cannot make up more than $1(10)\%$ of the MW halo (assuming the MW halo has a contracted Navarro Frenk White density profile fitted to Gaia DR2 and other data in Ref. [45]) [42]. There are also similar, but slightly weaker, constraints from OGLE's 20 years of SMC observations, with the six observed events being consistent with expectations from stars in the SMC or MW disc [84].

Niikura et al. [115] used OGLE microlensing observations towards the Galactic bulge to probe planetary mass COs. They found that most events were well-fit by microlensing by stellar populations and excluded $f > 0.1$ for $10^{-6} \lesssim M/M_\odot \lesssim 10^{-2}$. There was a distinct population of six ultra-short ($\sim$0.1 day) events. These events could be due to free-floating planets; however, they argued that these events are also consistent with Earth mass COs making up a few percent of the MW halo. From 2022-2024 OGLE carried out a high-cadence survey of the MCs, observing 35 million stars up to 21 times per night [116]. They only found one event, with Einstein radius crossing time $\sim$90 days, which allowed them to exclude COs with mass $10^{-8} \lesssim M/M_\odot \lesssim 0.01$ making up more than 1% of the MW halo.

### *3.5. Surveys Focused on M31*

Various collaborations have carried out so-called pixel microlensing surveys towards M31. Stars in M31 are too distant to be resolved individually, so instead microlensing surveys search for variations in the flux of the pixels of the image. Ref. [117] contains a review of pixel microlensing surveys towards M31 as of 2009.

In the early 2000s POINT-AGAPE [118] found 6 events, significantly more than the $\sim$1 they expected from self-lensing. They concluded that if the average mass of COs is $\sim 1(0.01)M_\odot$, then at 95% confidence they make up more than $20(8)$% of the MW halo. Subsequently, MEGA [119] and PLAN [120] both concluded (using detailed calculations of the detection efficiency and also more sophisticated mass models of M31 to calculate the self-lensing rate) that their observed event rates were broadly consistent with self lensing and constrained the MW halo fraction in Solar mass COs to be less than (20–30)%.

More recently high-cadence (2 min sampling interval) observations of M31 have been carried out using the Hyper Suprime-Cam (HSC) on the Subaru telescope [23,121]. Initial observations found one candidate event, which led to a constraint $f \lesssim 10^{-2}$ for $10^{-9} \lesssim M/M_\odot \lesssim 10^{-5}$ [23,23]. The finite size of the lensed stars reduces the magnification [68], and makes the constraint weaker than it would otherwise be, for $M \lesssim 10^{-7} M_\odot$ [23,122]. Very recently this work has been updated with additional data and improved analysis of the original data (in particular the inclusion of finite source size effects in the detection efficiency estimation) [121]. Twelve microlensing candidates have been identified, with 4 being classed as secure, high-significance detections. If these events are due to COs in the MW halo the corresponding mass and halo fraction are $M \sim (10^{-7} - 10^{-6})M_\odot$ and $f \sim 0.01 - 0.1$. Mróz and Udalski have, however, carried out an independent reanalysis of the data and argue that all 12 candidate events are in fact variable stars [123].

### *3.6. Kepler*

In the early 2010s Griest and collaborations searched for short timescale microlensing events in publicly available observations of nearby stars (designed to search for extra-Solar planets) by Kepler. Their final results [124], based on 2 years of data, excluded compact objects with $10^{-9} \lesssim M/M_\odot \lesssim 10^{-7}$ making up all of the MW halo.

### *3.7. Summary*

Figure 4 shows the final published parameter constraints on the halo fraction, $f$, and compact object mass, $M$, (assuming all compact objects have the same mass) from the surveys discussed in this section[7]. The solid lines denote exclusion limits, while the dot-dashed black line shows the envelope of the tightest constraint for each value of $M$. The dashed lines show allowed regions of parameter space. Table 2 contains a summary of the key features of the MACHO [6], EROS [14] and OGLE [22] LMC microlensing surveys.

See Table 1 of Ref. [31] for a more detailed comparison of stellar microlensing surveys (as of 2010).

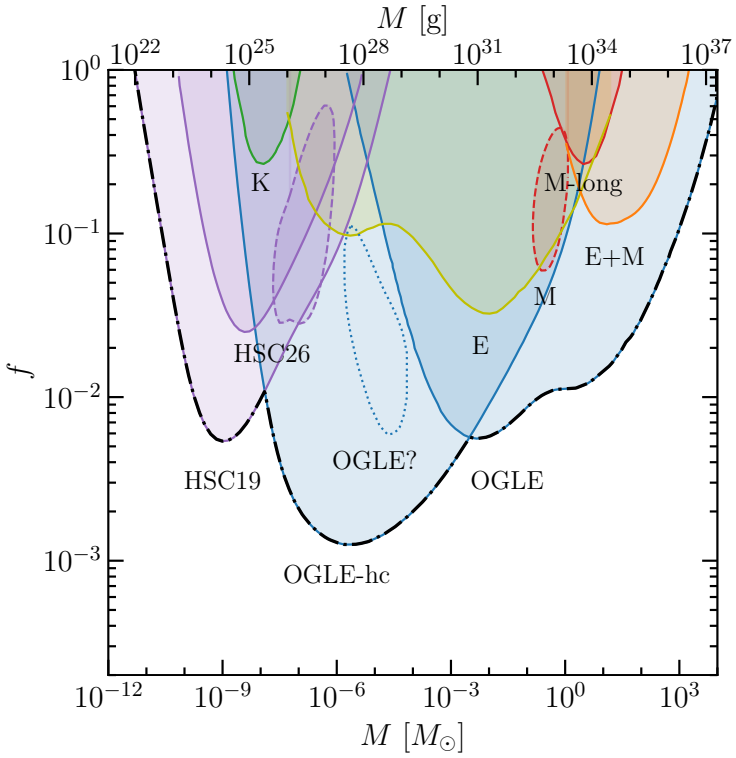



**Figure 4.** Constraints on the CO mass, $M$, and MW halo fraction, $f$, at 95% confidence, assuming all COs have the same mass. The solid lines denote exclusion limits, while the dot-dashed black line shows the envelope of the tightest constraint for each value of $M$. The dashed lines show allowed regions of parameter space. The exclusion limits are from EROS ('E') [14] (yellow), MACHO long timescale ('M-long') [100] (red), EROS plus MACHO long timescale ('E+M') [111] (orange), OGLE [22] and OGLE high-cadence ('OGLE-hc') [116] (blue), and Kepler ('K') [124] (green). The purple lines are from high-cadence observations of M31 using the Subaru-HSC. 'HSC19' shows the original exclusion limit [23] as calculated in Ref. [47], while 'HSC26' shows the exclusion limit from the latest analysis, under the assumption that none of the events observed are due to COs in the MW halo. The dashed line shows the allowed parameter values assuming that the 4 'secure' high-significance events are due to COs in the MW halo. The dashed red line shows the allowed parameter values from the 13 set A events in the final 5.7 year MACHO data set, as published in Ref. [6]. Subsequent observations indicate that some of these events are not microlensing (see Section 3.2 and Refs. [14,91] for discussion). The dotted blue line, labelled 'OGLE?', shows the parameter values found assuming that the ultra-short duration events observed towards the Galactic bulge by OGLE are due to COs in the MW halo [115]. This plot was made using a modified version of Kavanagh's PBHBounds [125].

**Table 2.** A summary of the main features of the MACHO [6], EROS [14] and OGLE [22] LMC microlensing surveys. The 13 MACHO events are from their tighter selection criteria A. Four of these events have subsequently been found to likely be variable stars; see Refs. [14,91] and Section 3.2. The 13 events listed for OGLE are those found using their automated search pipeline, and used for their halo fraction constraints; see Section 3.4.

| Survey | Duration (Years) | Field of View ($deg^2$) | Number of Stars, $N_\star$ (Million) | Number of Events, $N_{obs}$ |
|---|---|---|---|---|
| MACHO | 5.7 | 14 | 12 | 13 |
| EROS | ∼12 | 88 (EROS-2) | ∼25 (EROS-2) | 1 |
| OGLE | ∼20 | 105 (OGLE-IV) | 78.7 (OGLE-IV) | 13 |

## 4. Future

### *4.1. Observations*

In the near future new telescopes will be able to carry out next generation microlensing surveys. The Nancy Grace Roman Space Telescope (formerly known as WFIRST) has excellent resolution, which will reduce the effects of blending and allow the measurement of finite source effects. It will carry out high-cadence observations, as required to detect short timescale events and probe light CO. The ground-based Vera C. Rubin Observatory (formerly known as the Large Synoptic Survey Telescope) will carry out a long-duration wide-field survey. It will have high sensitivity to long timescale events and hence intermediate and high mass CO. Telescopes with high spatial resolution, capable of high-precision astrometry, will be able to carry out astrometric microlensing measurements and probe the angular Einstein radius (see Section 2.4).

To probe CO DM with the Roman Space Telescope's Galactic Bulge Time Domain Survey it will be necessary to discriminate events due to CO in the MW halo from events due to astrophysical objects in the luminous components of the MW. Following early work in Ref. [126], Ref. [127] showed that it will be possible to discriminate planetary-mass CO DM from free-floating planets, and probe halo fractions $f \sim 10^{-3} - 10^{-4}$ using just the timescales of (photometric) microlensing events. Ref. [128] showed that this survey could probe $f \sim 10^{-3}$ for $10^{-1} \lesssim M/M_\odot \lesssim 10^2$ *if* it is possible to distinguish CO DM and stellar lenses using the joint distributions of the timescales and angular Einstein radii of events. If it is not possible to do this then the sensitivity will be reduced to $f \sim 10^{-1}$, weaker than existing OGLE limits in this mass range [22]. Similar constraints may also be possible using the Rubin Observatory [129]. With improved understanding of backgrounds, Gaia time-series data could probe halo fractions down to $f \sim 10^{-3}$ for multi-Solar mass CO DM [130]; see also Ref. [79]. The thirty-metre class, Extremely Large Telescopes, will also be able to probe CO DM via astrometric microlensing [131]. Combining photometric and astrometric microlensing data would aid the detection and characterization of events [132]. In all cases, correctly identifying events and minimizing the false positive rate will be crucial (as we have seen for previous surveys in Section 3). See Ref. [133] for work in this direction.

### *4.2. Theory*

As discussed in Section 2.2, uncertainties in the DM distribution lead to uncertainties in the differential event rate and hence the constraints on the halo fraction. If the DM is smoothly distributed, the most significant uncertainty is the dependence of the rate of short-timescale events, and hence the constraints on $f$ for large masses, on the local velocity distribution [52]. In the case of PBHs, if a significant fraction is in compact clusters, such that the cluster as a whole lenses, the constraints would change significantly [50]. Understanding the present day spatial distribution of PBHs formed from realistic density perturbation distributions (i.e., how many PBHs are in clusters, and what are their properties? How many PBHs are in binaries, and what are their properties?) is a major outstanding challenge.

## 5. Summary

We have explored how stellar microlensing surveys probe compact object dark matter, in particular primordial black holes. Early indications from the MACHO collaboration that a significant fraction of the Milky Way halo could be in the form of roughly Solar Mass COs [5,6] were not confirmed by EROS [14] or OGLE [22]. Long-duration [22] and high-cadence [23,116] observations have extended the range of CO masses probed by microlensing. Under the standard assumptions outlined in Section 2, collectively these surveys exclude COs with mass $10^{-11} \lesssim M/M_\odot \lesssim 10^4$ making up all of the DM in the MW, while those in the mass range $10^{-10} \lesssim M/M_\odot \lesssim 1$ can make up less than one percent. Further theoretical work is required to ascertain how robust the standard

assumptions regarding the CO distribution are. For PBHs a key question is whether a significant fraction are in compact clusters. Future observations, in particular astrometric ones using the Roman Telescope and Rubin Observatory can potentially probe CO dark matter down to $f \sim 10^{-3} - 10^{-4}$. However further work is required to develop techniques for discriminating CO dark matter-induced lensing events from backgrounds, including lensing events due to known astrophysical objects, such as stars and planets.

**Funding:** This research was supported by an STFC Consolidated Grant [Grant No. ST/T000732/1] and a Leverhulme Trust Research Fellowship [Grant No. RF-2025-282].

**Data Availability Statement:** No new data were created or analysed in this study. Data sharing is not applicable to this article.

**Conflicts of Interest:** The author declares no conflicts of interest.

## Abbreviations

The following abbreviations are used in this manuscript:

| | |
|---|---|
| CO | Compact Object |
| DM | Dark Matter |
| DIA | Difference Image Analysis |
| LMC | Large Magellanic Cloud |
| MC | Magellanic Cloud |
| MW | Milky Way |
| PBH | Primordial Black Hole |
| SMC | Small Magellanic Cloud |

## Notes

[1] Throughout, we use COs when covering material that applies to compact objects in general and PBHs for material that is specific to primordial black holes.

[2] We do not cover constraints on CO DM [24,25] from supermagnified stars (a star in a galaxy that is magnified by a large factor by lensing by a galaxy cluster, with the star then magnified further by microlensing by a CO) [26].

[3] These advantages are well known in the observational microlensing community but are hard to find original sources for.

[4] There have been changes to some of best-fit parameter values; for instance, the Solar radius has been measured as $r_0 = (8.18 \pm 0.01 \pm 0.02)$ kpc by the GRAVITY collaboration [35]. However, these changes have a smaller effect on the differential event rate than uncertainties in the density profile.

[5] The event numbering reflects the fact that events 2 and 3 in the 1-year data were subsequently rejected, and a further 8 candidate events were classed as supernovae in background galaxies.

[6] Event 23 has varied again and is likely a variable star; see discussion above and Refs. [14,86,92].

[7] Results from M31 surveys, other than HSC, are not shown. These surveys quoted approximate allowed or excluded values for the halo fraction, but they did not publish exclusion limit curves or allowed regions of parameter space.

## References

1. Einstein, A. Lens-like Action of a Star by the Deviation of Light in the Gravitational Field. *Science* **1936**, *84*, 506–507. [CrossRef]
2. Paczyński, B. Gravitational microlensing by the galactic halo. *Astrophys. J.* **1986**, *304*, 1–5. [CrossRef]
3. Aubourg, E.; Bareyre, P.; Bréhin, S.; Gros, M.; Lachièze-Rey, M.; Laurent, B.; Lesquoy, E.; Magneville, C.; Milsztajn, A.; Moscoso, L.; et al. Evidence for gravitational microlensing by dark objects in the Galactic halo. *Nature* **1993**, *365*, 623–625. [CrossRef]
4. Alcock, C.; Akerlof, C.W.; Allsman, R.A.; Axelrod, T.S.; Bennett, D.P.; Chan, S.; Cook, K.H.; Freeman, K.C.; Griest, K.; Marshall, S.L.; et al. Possible Gravitational Microlensing of a Star in the Large Magellanic Cloud. *Nature* **1993**, *365*, 621–623. [CrossRef]
5. Alcock, C.; Allsman, R.A.; Alves, D.; Axelrod, T.S.; Becker, A.C.; Bennett, D.P.; Cook, K.H.; Freeman, K.C.; Griest, K.; Guern, J.; et al. The MACHO project LMC microlensing results from the first two years and the nature of the galactic dark halo. *Astrophys. J.* **1997**, *486*, 697–726. [CrossRef]
6. Alcock, C.; Allsman, R.A.; Alves, D.R.; Axelrod, T.S.; Becker, A.C.; Bennett, D.P.; Cook, K.H.; Dalal, N.; Drake, A.J.; Freeman, K.C.; et al. The MACHO project: Microlensing results from 5.7 years of LMC observations. *Astrophys. J.* **2000**, *542*, 281–307. [CrossRef]

7. Fields, B.D.; Freese, K.; Graff, D.S. Chemical abundance constraints on white dwarfs as halo dark matter. *Astrophys. J.* **2000**, *534*, 265–276. [CrossRef]
8. Yokoyama, J. Formation of MACHO primordial black holes in inflationary cosmology. *Astron. Astrophys.* **1997**, *318*, 673.
9. Jedamzik, K. Could MACHOS be primordial black holes formed during the QCD epoch? *Phys. Rept.* **1998**, *307*, 155–162. [CrossRef]
10. Zel'dovich, Y.B.; Novikov, I.D. The Hypothesis of Cores Retarded during Expansion and the Hot Cosmological Model. *Sov. Astron.* **1967**, *10*, 602.
11. Hawking, S. Gravitationally collapsed objects of very low mass. *Mon. Not. Roy. Astron. Soc.* **1971**, *152*, 75. [CrossRef]
12. Ansari, R.; Cavalier, F.; Moniez, M.; Aubourg, E.; Bareyre, P.; Brehin, S.; Gros, M.; Lachieze-Rey, M.; Laurent, B.; Lesquoy, E.; et al. Observational limits on the contribution of sub-stellar and stellar objects to the galactic halo. *Astron. Astrophys.* **1996**, *314*, 94–103. [CrossRef]
13. Lasserre, T.; Afonso, C.; Albert, J.N.; Andersen, J.; Ansari, R.; Aubourg, É.; Bareyre, P.; Bauer, F.; Beaulieu, J.P.; Blanc, G.; et al. Not enough stellar mass Machos in the Galactic halo. *Astron. Astrophys.* **2000**, *355*, L39–L42. [CrossRef]
14. Tisserand, P.; Le Guillou, L.; Afonso, C.; Albert, J.N.; Andersen, J.; Ansari, R.; Aubourg, É.; Bareyre, P.; Beaulieu, J.P.; Charlot, X.; et al. Limits on the Macho content of the Galactic Halo from the EROS-2 Survey of the Magellanic Clouds. *Astron. Astrophys.* **2007**, *469*, 387–404. [CrossRef]
15. Wyrzykowski, L.; Kozłowski, S.; Skowron, J.; Belokurov, V.; Smith, M.C.; Udalski, A.; Szymański, M.K.; Kubiak, M.; Pietrzyński, G.; Soszyński, I.; et al. The OGLE View of Microlensing towards the Magellanic Clouds. I. A Trickle of Events in the OGLE-II LMC data. *Mon. Not. Roy. Astron. Soc.* **2009**, *397*, 1228–1242. [CrossRef]
16. Wyrzykowski, L.; Skowron, J.; Kozłowski, S.; Udalski, A.; Szymański, M.K.; Kubiak, M.; Pietrzyński, G.; Soszyński, I.; Szewczyk, O.; Ulaczyk, K.; et al. The OGLE View of Microlensing towards the Magellanic Clouds. IV. OGLE-III SMC Data and Final Conclusions on MACHOs. *Mon. Not. Roy. Astron. Soc.* **2011**, *416*, 2949. [CrossRef]
17. Abbott, B.P.; Abbott, R.; Abbott, T.D.; Abernathy, M.R.; Acernese, F.; Ackley, K.; Adams, C.; Adams, T.; Addesso, P.; Adhikari, R.X.; et al. Observation of Gravitational Waves from a Binary Black Hole Merger. *Phys. Rev. Lett.* **2016**, *116*, 061102. [CrossRef]
18. Bird, S.; Cholis, I.; Muñoz, J.B.; Ali-Haïmoud, Y.; Kamionkowski, M.; Kovetz, E.D.; Raccanelli, A.; Riess, A.G. Did LIGO detect dark matter? *Phys. Rev. Lett.* **2016**, *116*, 201301. [CrossRef] [PubMed]
19. Clesse, S.; García-Bellido, J. The clustering of massive Primordial Black Holes as Dark Matter: Measuring their mass distribution with Advanced LIGO. *Phys. Dark Univ.* **2017**, *15*, 142–147. [CrossRef]
20. Sasaki, M.; Suyama, T.; Tanaka, T.; Yokoyama, S. Primordial Black Hole Scenario for the Gravitational-Wave Event GW150914. *Phys. Rev. Lett.* **2016**, *117*, 061101. Erratum in *Phys. Rev. Lett.* **2018**, *121*, 059901. [CrossRef] [PubMed]
21. Carr, B.; Kuhnel, F.; Sandstad, M. Primordial Black Holes as Dark Matter. *Phys. Rev. D* **2016**, *94*, 083504. [CrossRef]
22. Mróz, P.; Udalski, A.; Szymański, M.K.; Kapusta, M.; Soszyński, I.; Wyrzykowski, Ł.; Pietrukowicz, P.; Kozłowski, S.; Poleski, R.; Skowron, J.; et al. Microlensing Optical Depth and Event Rate toward the Large Magellanic Cloud Based on 20 yr of OGLE Observations. *Astrophys. J. Suppl.* **2024**, *273*, 4. [CrossRef]
23. Niikura, H.; Takada, M.; Yasuda, N.; Lupton, R.H.; Sumi, T.; More, S.; Kurita, T.; Sugiyama, S.; More, A.; Oguri, M.; et al. Microlensing constraints on primordial black holes with Subaru/HSC Andromeda observations. *Nat. Astron.* **2019**, *3*, 524–534. [CrossRef]
24. Diego, J.M.; Kaiser, N.; Broadhurst, T.; Kelly, P.L.; Rodney, S.; Morishita, T.; Oguri, M.; Ross, T.W.; Zitrin, A.; Jauzac, M.; et al. Dark Matter under the Microscope: Constraining Compact Dark Matter with Caustic Crossing Events. *Astrophys. J.* **2018**, *857*, 25. [CrossRef]
25. Müller, C.V.; Miralda-Escudé, J. Limits on dark matter compact objects implied by supermagnified stars in lensing clusters. *Mon. Not. Roy. Astron. Soc.* **2024**, *536*, 1579–1585. [CrossRef]
26. Venumadhav, T.; Dai, L.; Miralda-Escudé, J. Microlensing of Extremely Magnified Stars near Caustics of Galaxy Clusters. *Astrophys. J.* **2017**, *850*, 49. [CrossRef]
27. Carr, B.J.; Green, A.M. The History of Primordial Black Holes. *arXiv* **2025**, arXiv:2406.05736.
28. Green, A.M.; Kavanagh, B.J. Primordial Black Holes as a dark matter candidate. *J. Phys. G* **2021**, *48*, 043001. [CrossRef]
29. Carr, B.; Iovino, A.J.; Perna, G.; Vaskonen, V.; Veermäe, H. Primordial black holes: Constraints, potential evidence and prospects. *arXiv* **2026**, arXiv:2601.06024. [CrossRef]
30. Mao, S. Astrophysical applications of gravitational microlensing. *Res. Astron. Astrophys.* **2012**, *12*, 947–972. [CrossRef]
31. Moniez, M. Microlensing as a probe of the Galactic structure: 20 years of microlensing optical depth studies. *Gen. Rel. Grav.* **2010**, *42*, 2047–2074. [CrossRef]
32. Jetzer, P. Limits on compact baryonic dark matter from gravitational microlensing. *Phys. Scr.* **2014**, *8*, 084009. [CrossRef]
33. Refsdal, S. The gravitational lens effect. *Mon. Not. Roy. Astron. Soc.* **1964**, *128*, 295. [CrossRef]
34. Pietrzyński, G.; Graczyk, D.; Gallenne, A.; Gieren, W.; Thompson, I.B.; Pilecki, B.; Karczmarek, P.; Górski, M.; Suchomska, K.; Taormina, M.; et al. A distance to the Large Magellanic Cloud that is precise to one per cent. *Nature* **2019**, *567*, 200–203. [CrossRef]

35. GRAVITY Collaboration; Abuter, R.; Amorim, A.; Bauböck, M.; Berger, J.P.; Bonnet, H.; Brandner, W.; Clénet, Y.; Coudé Du Foresto, V.; de Zeeuw, P.T.; et al. A geometric distance measurement to the Galactic center black hole with 0.3% uncertainty. *Astron. Astrophys.* **2019**, *625*, L10. [CrossRef]
36. Griest, K. Galactic Microlensing as a Method of Detecting Massive Compact Halo Objects. *Astrophys. J.* **1991**, *366*, 412–421. [CrossRef]
37. Alcock, C.; Allsman, R.A.; Axelrod, T.S.; Bennett, D.P.; Cook, K.H.; Freeman, K.C.; Griest, K.; Guern, J.A.; Lehner, M.J.; Marshall, S.L.; et al. The MACHO project first year LMC results: The Microlensing rate and the nature of the galactic dark halo. *Astrophys. J.* **1996**, *461*, 84. [CrossRef] [PubMed]
38. Zhao, H.; Rich, R.M.; Spergel, D.N. A consistent microlensing model for the galactic bar. *Mon. Not. Roy. Astron. Soc.* **1996**, *282*, 175. [CrossRef]
39. Mao, S.d.; Paczyński, B. Mass determination with gravitational microlensing. *Astrophys. J.* **1996**, *473*, 57. [CrossRef]
40. Sahu, K.C. Stars within the Large Magellanic Cloud as potential lenses for observed microlensing events. *Nature* **1994**, *370*, 275. [CrossRef]
41. Gyuk, G.; Dalal, N.; Griest, K. Selflensing models of the lmc. *Astrophys. J.* **2000**, *535*, 90–103. [CrossRef]
42. Mróz, P.; Udalski, A.; Szymański, M.K.; Soszyński, I.; Wyrzykowski, Ł.; Pietrukowicz, P.; Kozłowski, S.; Poleski, R.; Skowron, J.; Skowron, D.; et al. No massive black holes in the Milky Way halo. *Nature* **2024**, *632*, 749–751. [CrossRef]
43. Calchi Novati, S.; Mancini, L. Microlensing towards the Large Magellanic Cloud: Self-lensing for OGLE-II and OGLE-III. *Mon. Not. Roy. Astron. Soc.* **2011**, *416*, 1292–1301. [CrossRef]
44. Han, C.; Gould, A.P. Stellar contribution to the Galactic bulge microlensing optical depth. *Astrophys. J.* **2003**, *592*, 172–175. [CrossRef]
45. Cautun, M.; Benitez-Llambay, A.; Deason, A.J.; Frenk, C.S.; Fattahi, A.; Gómez, F.A.; Grand, R.J.J.; Oman, K.A.; Navarro, J.F.; Simpson, C.M. The Milky Way total mass profile as inferred from Gaia DR2. *Mon. Not. Roy. Astron. Soc.* **2020**, *494*, 4291–4313. [CrossRef]
46. Carr, B.; Raidal, M.; Tenkanen, T.; Vaskonen, V.; Veermäe, H. Primordial black hole constraints for extended mass functions. *Phys. Rev. D* **2017**, *96*, 023514. [CrossRef]
47. Croon, D.; McKeen, D.; Raj, N.; Wang, Z. Subaru-HSC through a different lens: Microlensing by extended dark matter structures. *Phys. Rev. D* **2020**, *102*, 083021. [CrossRef]
48. Hawkins, M.R.S. A new look at microlensing limits on dark matter in the Galactic halo. *Astron. Astrophys.* **2015**, *575*, A107. [CrossRef]
49. Green, A.M. Astrophysical uncertainties on stellar microlensing constraints on multi-Solar mass primordial black hole dark matter. *Phys. Rev. D* **2017**, *96*, 043020. [CrossRef]
50. Calcino, J.; Garcia-Bellido, J.; Davis, T.M. Updating the MACHO fraction of the Milky Way dark halowith improved mass models. *Mon. Not. Roy. Astron. Soc.* **2018**, *479*, 2889–2905. [CrossRef]
51. Garcia-Bellido, J.; Hawkins, M. Reanalysis of the MACHO Constraints on PBH in the Light of Gaia DR3 Data. *Universe* **2024**, *10*, 449. [CrossRef]
52. Green, A.M. Primordial black hole stellar microlensing constraints: Understanding their dependence on the density and velocity distributions. *J. Cosmol. Astropart. Phys.* **2025**, *04*, 023. [CrossRef]
53. Sahu, K.C.; Sahu, M.S. Spectroscopy of MACHO 97-smc-1: Self-lensing within the smc. *Astrophys. J. Lett.* **1998**, *508*, L147. [CrossRef]
54. Palanque-Delabrouille, N.; Afonso, C.; Albert, J.N.; Andersen, J.; Ansari, R.; Aubourg, E.; Bareyre, P.; Bauer, F.; Beaulieu, J.P.; Bouquet, A.; et al. Microlensing towards the small magellanic cloud. eros 2 first year survey . *Astron. Astrophys.* **1998**, *332*, 1–9.
55. Graff, D.S.; Gardiner, L.T. Microlensing in the Small Magellanic Cloud: Lessons from an N-body Simulation. *Mon. Not. Roy. Astron. Soc.* **1999**, *307*, 577. [CrossRef]
56. Povick, J.T.; Nidever, D.L.; Massana, P.; Majewski, S.R.; Lu, Y.; Cioni, M.R.L.; Geisler, D.; Mészáros, S.; Nitschelm, C.; Almeida, A.; et al. Revealing the chemical structure of the Magellanic Clouds with APOGEE. III. Abundance gradients of the Small Magellanic Cloud. *Mon. Not. Roy. Astron. Soc.* **2025**, *544*, 430–456. [CrossRef]
57. Crotts, A.P.S. M31: A Unique laboratory for gravitational microlensing. *Astrophys. J. Lett.* **1992**, *399*, L43–L46. [CrossRef] [PubMed]
58. Baillon, P.; Bouquet, A.; Giraud-Heraud, Y.; Kaplan, J. Detection of brown dwarfs by the micro-lensing of unresolved stars. *Astron. Astrophys.* **1993**, *277*, 1–9. [CrossRef]
59. Kerins, E.; Carr, B.J.; Evans, N.W.; Hewett, P.C.; Lastennet, E.; Du, Y.L.; Melchior, A.L.; Smartt, S.J.; Valls-Gabaud, D. Theory of pixel lensing towards m31 I: The density contribution and mass of machos. *Mon. Not. Roy. Astron. Soc.* **2001**, *323*, 13. [CrossRef]
60. Baltz, E.A.; Gyuk, G.; Crotts, A. Event rates and timescale distributions from realistic microlensing models of M31. *Astrophys. J.* **2003**, *582*, 30. [CrossRef]

61. Afshordi, N.; McDonald, P.; Spergel, D.N. Primordial black holes as dark matter: The Power spectrum and evaporation of early structures. *Astrophys. J. Lett.* **2003**, *594*, L71–L74. [CrossRef]
62. Inman, D.; Ali-Haïmoud, Y. Early structure formation in primordial black hole cosmologies. *Phys. Rev. D* **2019**, *100*, 083528. [CrossRef]
63. Jedamzik, K. Primordial Black Hole Dark Matter and the LIGO/Virgo observations. *J. Cosmol. Astropart. Phys.* **2020**, *09*, 022. [CrossRef]
64. Petač, M.; Lavalle, J.; Jedamzik, K. Microlensing constraints on clustered primordial black holes. *Phys. Rev. D* **2022**, *105*, 083520. [CrossRef]
65. Gorton, M.; Green, A.M. Effect of clustering on primordial black hole microlensing constraints. *J. Cosmol. Astropart. Phys.* **2022**, *08*, 035. [CrossRef]
66. Atal, V.; Germani, C. The role of non-gaussianities in Primordial Black Hole formation. *Phys. Dark Univ.* **2019**, *24*, 100275. [CrossRef]
67. Young, S.; Byrnes, C.T. Initial clustering and the primordial black hole merger rate. *J. Cosmol. Astropart. Phys.* **2020**, *03*, 004. [CrossRef]
68. Witt, H.J.; Mao, S. Can Lensed Stars Be Regarded as Pointlike for Microlensing by MACHOs? *Astrophys. J.* **1994**, *430*, 505. [CrossRef]
69. Gould, A. Proper Motions of MACHOs. *Astrophys. J. Lett.* **1994**, *421*, L71. [CrossRef] [PubMed]
70. Sasaki, M.; Suyama, T.; Tanaka, T.; Yokoyama, S. Primordial black holes—perspectives in gravitational wave astronomy. *Class. Quant. Grav.* **2018**, *35*, 063001. [CrossRef]
71. Gould, A. Extending the MACHO Search to approximately 10 6 M sub sun. *Astrophys. J.* **1992**, *392*, 442. [CrossRef]
72. Griest, K.; Hu, W. Effect of Binary Sources on the Search for Massive Astrophysical Compact Halo Objects via Microlensing. *Astrophys. J.* **1992**, *397*, 362. [CrossRef]
73. Mao, S.; Paczynski, B. Gravitational Microlensing by Double Stars and Planetary Systems. *Astrophys. J. Lett.* **1991**, *374*, L37. [CrossRef]
74. Sugiyama, S.; Kurita, T.; Takada, M. On the wave optics effect on primordial black hole constraints from optical microlensing search. *Mon. Not. Roy. Astron. Soc.* **2020**, *493*, 3632–3641. [CrossRef]
75. Montero-Camacho, P.; Fang, X.; Vasquez, G.; Silva, M.; Hirata, C.M. Revisiting constraints on asteroid-mass primordial black holes as dark matter candidates. *J. Cosmol. Astropart. Phys.* **2019**, *08*, 031. [CrossRef]
76. Boutreux, T.; Gould, A. Monte Carlo Simulations of MACHO Parallaxes from a Satellite. *Astrophys. J.* **1996**, *462*, 705. [CrossRef]
77. Miyamoto, M.; Yoshii, Y. Astrometry for Determining the MACHO Mass and Trajectory. *Astron. J.* **1995**, *110*, 1427. [CrossRef]
78. Walker, M.A. Microlensed Image Motions. *Astrophys. J. Lett.* **1995**, *453*, 37. [CrossRef]
79. Belokurov, V.A.; Evans, N.W. Astrometric microlensing with the GAIA satellite. *Mon. Not. Roy. Astron. Soc.* **2002**, *331*, 649–665. [CrossRef]
80. Miralda-Escude, J. Microlensing Events from Measurements of the Deflection. *Astrophys. J. Lett.* **1996**, *470*, L113. [CrossRef]
81. Dominik, M.; Sahu, K.C. Astrometric Microlensing of Stars. *Astrophys. J. Lett.* **2000**, *534*, 213–226. [CrossRef]
82. Alcock, C.; Allsman, R.A.; Alves, D.R.; Axelrod, T.S.; Becker, A.C.; Bennett, D.P.; Cook, K.H.; Drake, A.J.; Freeman, K.C.; Geha, M.; et al. The MACHO Project: Microlensing Detection Efficiency. *Astrophys. J.* **2001**, *136*, 439–462. [CrossRef]
83. Zebrun, K.; Soszynski, I.; Wozniak, P.R.; Udalski, A.; Kubiak, M.; Szymanski, M.; Pietrzynski, G.; Szewczyk, O.; Wyrzykowski, L. The optical gravitational lensing experiment. difference image analysis of lmc and smc data. the catalog. *Acta Astron.* **2001**, *51*, 317–329.
84. Mróz, P.; Udalski, A.; Szymański, M.K.; Soszyński, I.; Pietrukowicz, P.; Kozłowski, S.; Poleski, R.; Skowron, J.; Skowron, D.; Ulaczyk, K.; et al. Microlensing optical depth, event rate, and limits on compact objects in dark matter based on 20 years of OGLE observations of the Small Magellanic Cloud. *Astrophys. J. Suppl. Ser.* **2025**, *280*, 49. [CrossRef]
85. Griest, K.; Thomas, C.L. Contamination in the MACHO dataset and the puzzle of LMC microlensing. *Mon. Not. Roy. Astron. Soc.* **2005**, *359*, 464–468. [CrossRef]
86. Bennett, D.P.; Becker, A.C.; Tomaney, A. Photometric Confirmation of MACHO Large Magellanic Cloud Microlensing Events. *Astrophys. J.* **2005**, *631*, 301–311. [CrossRef]
87. Smith, M.C.; Wozniak, P.; Mao, S.; Sumi, T. Blending in Gravitational Microlensing Experiments: Source Confusion and Related Systematics. *Mon. Not. Roy. Astron. Soc.* **2007**, *380*, 805. [CrossRef]
88. Bennett, D.P.; Alcock, C.; Allsman, R.A.; Alves, D.; Axelrod, T.S.; Becker, A.; Cook, K.H.; Freeman, K.C.; Griest, K.; Guern, J.; et al. A Binary lensing event toward the LMC: Observations and dark matter implications. *Nucl. Phys. B Proc. Suppl.* **1996**, *51*, 152–156. [CrossRef]
89. Alcock, C.; Allsman, R.A.; Alves, D.; Axelrod, T.S.; Becker, A.C.; Bennett, D.P.; Cook, K.H.; Freeman, K.C.; Griest, K.; Guern, J.; et al. The MACHO Project: Limits on Planetary Mass Dark Matter in the Galactic Halo from Gravitational Microlensing. *Astrophys. J.* **1996**, *471*, 774. [CrossRef]

90. Alcock, C.; Allsman, R.A.; Alves, D.; Ansari, R.; Aubourg, É.; Axelrod, T.S.; Bareyre, P.; Beaulieu, J.P.; Becker, A.C.; Bennett, D.P.; et al. EROS and MACHO Combined Limits on Planetary-Mass Dark Matter in the Galactic Halo. *Astrophys. J. Lett.* **1998**, *499*, L9–L12. [CrossRef]
91. Mróz, P.; Udalski, A.; Szymański, M.K.; Soszyński, I.; Wyrzykowski, Ł.; Pietrukowicz, P.; Kozłowski, S.; Poleski, R.; Skowron, J.; Skowron, D.; et al. Eppur non si trovano: Comments on the Primordial Black Hole Limits in the Galactic Halo. *arXiv* **2025**, arXiv:2510.20005. [CrossRef]
92. Wyrzykowski, Ł.; Kozłowski, S.; Skowron, J.; Udalski, A.; Szymański, M.K.; Kubiak, M.; Pietrzyński, G.; Soszyński, I.; Szewczyk, O.; Ulaczyk, K.; et al. The OGLE view of microlensing towards the Magellanic Clouds—III. Ruling out subsolar MACHOs with the OGLE-III LMC data. *Mon. Not. Roy. Astron. Soc.* **2011**, *413*, 493–508. [CrossRef]
93. Drake, A.J.; Cook, K.H.; Keller, S.C. Resolving the nature of the LMC microlensing event LMC-5. *Astrophys. J. Lett.* **2004**, *607*, L29–L32. [CrossRef]
94. Gould, A. Resolution of the macho-lmc-5 puzzle: The jerk-parallax microlens degeneracy. *Astrophys. J.* **2004**, *606*, 319–325. [CrossRef]
95. Gould, A.P.; Bahcall, J.N.; Flynn, C. M dwarfs from Hubble Space Telescope star counts. 3. The Groth strip. *Astrophys. J.* **1997**, *482*, 913. [CrossRef]
96. Alcock, C.; Allsman, R.A.; Alves, D.R.; Axelrod, T.S.; Becker, A.C.; Bennett, D.P.; Cook, K.H.; Drake, A.J.; Freeman, K.C.; Geha, M.; et al. MACHO 96-LMC-2: Lensing of a Binary Source in the Large Magellanic Cloud and Constraints on the Lensing Object. *Astrophys. J.* **2001**, *552*, 259–267. [CrossRef]
97. Dominik, M.; Hirshfeld, A.C. The binary nature of an observed dark galatic object. *Astron. Astrophys.* **1994**, *289*, L31–L33.
98. Dominik, M.; Hirshfeld, A.C. Evidence for a binary lens in the MACHO LMC No. 1 microlensing event. *Astron. Astrophys.* **1996**, *313*, 841–850.
99. Kallivayalil, N.; Patten, B.M.; Marengo, M.; Alcock, C.; Werner, M.W.; Fazio, G.G. Identification of the Microlens in Event MACHO-LMC-20. *Astrophys. J. Lett.* **2006**, *652*, L97–L100. [CrossRef]
100. Allsman, R.A.; Alves, D.R.; Axelrod, T.S.; Becker, A.C.; Bennett, D.P.; Cook, K.H.; Dalal, N.; Drake, A.J.; Geha, M.; Griest, K. MACHO project limits on black hole dark matter in the 1-30 solar mass range. *Astrophys. J. Lett.* **2001**, *550*, L169. [CrossRef]
101. Belokurov, V.; Evans, N.W.; Le Du, Y. Lightcurve classification in massive variability surveys 2: Transients towards the Large Magellanic Cloud. *Mon. Not. Roy. Astron. Soc.* **2004**, *352*, 233. [CrossRef]
102. Bennett, D.P. Large Magellanic Cloud Microlensing Optical Depth with Imperfect Event Selection. *Astrophys. J.* **2005**, *633*, 906–913. [CrossRef]
103. Hawkins, M.R.S.; García-Bellido, J. A critical analysis of the recent OGLE limits on stellar mass primordial black holes in the halo of the Milky Way. *arXiv* **2025**, arXiv:2509.05400. [CrossRef]
104. Alcock, C.; Allsman, R.A.; Alves, D.; Axelrod, T.S.; Becker, A.C.; Bennett, D.P.; Cook, K.H.; Freeman, K.C.; Griest, K.; Keane, M.J.; et al. First Detection of a Gravitational Microlensing Candidate toward the Small Magellanic Cloud. *Astrophys. J. Lett.* **1997**, *491*, L11–L13. [CrossRef]
105. Udalski, A.; Szymanski, M.; Kubiak, M.; Pietrzynski, G.; Wozniak, P.; Zebrun, K. Optical Gravitational Lensing Experiment. Photometry of the MACHO-SMC-1 Microlensing Candidate. *Acta Astron.* **1997**, *47*, 431–436. [CrossRef]
106. Alcock, C.; Allsman, R.A.; Alves, D.; Axelrod, T.S.; Becker, A.C.; Bennett, D.P.; Cook, K.H.; Drake, A.J.; Freeman, K.C.; Griest, K.; et al. Discovery and Characterization of a Caustic Crossing Microlensing Event in the Small Magellanic Cloud. *Astrophys. J.* **1999**, *518*, 44–49. [CrossRef]
107. Renault, C.; Afonso, C.; Aubourg, E.; Bareyre, P.; Bauer, F.; Brehin, S.; Coutures, C.; Gaucherel, C.; Glicenstein, J.F.; Goldman, B.; et al. Observational limits on MACHOS in the Galactic Halo. *Astron. Astrophys.* **1997**, *324*, L69–L72.
108. Renault, C.; Aubourg, E.; Bareyre, P.; Brehin, S.; Gros, M.; Lachieze-Rey, M.; Laurent, B.; Lesquoy, E.; Magneville, C.; Milsztajn, A.; et al. Search for planetary mass objects in the Galactic halo through microlensing. *Astron. Astrophys.* **1998**, *329*, 522–537.
109. Afonso, C.; Alard, C.; Albert, J.N.; Andersen, J.; Ansari, R.; Aubourg, É.; Bareyre, P.; Bauer, F.; Beaulieu, J.P.; Bouquet, A.; et al. Microlensing towards the Small Magellanic Cloud EROS 2 two-year analysis. *Astron. Astrophys.* **1999**, *344*, L63–L66.
110. Afonso, C.; Albert, J.N.; Andersen, J.; Ansari, R.; Aubourg, É.; Bareyre, P.; Beaulieu, J.P.; Blanc, G.; Charlot, X.; Couchot, F.; et al. Limits on Galactic dark matter with 5 years of EROS SMC data. *Astron. Astrophys.* **2003**, *400*, 951–956. [CrossRef]
111. Blaineau, T.; Moniez, M.; Afonso, C.; Albert, J.N.; Ansari, R.; Aubourg, E.; Coutures, C.; Glicenstein, J.F.; Goldman, B.; Hamadache, C.; et al. New limits from microlensing on Galactic black holes in the mass range 10 $M_\odot$ < M < 1000 $M_\odot$. *Astron. Astrophys.* **2022**, *664*, A106. [CrossRef]
112. Soszyński, I. Three decades of the OGLE survey. *Contrib. Astron. Obs. Skaln. Pleso* **2024**, *54*, 234–248. [CrossRef]
113. Wyrzykowski, L.; Kozłowski, S.; Skowron, J.; Belokurov, V.; Smith, M.C.; Udalski, A.; Szymański, M.K.; Kubiak, M.; Pietrzyński, G.; Soszyński, I.; et al. The OGLE View of Microlensing towards the Magellanic Clouds. II. OGLE-II SMC data. *Mon. Not. Roy. Astron. Soc.* **2010**, *407*, 189–200. [CrossRef]

114. Dong, S.; Udalski, A.; Gould, A.; Reach, W.T.; Christie, G.W.; Boden, A.F.; Bennett, D.P.; Fazio, G.; Griest, K.; Szymański, M.K.; et al. First Space-Based Microlens Parallax Measurement: Spitzer Observations of OGLE-2005-SMC-001. *Astrophys. J.* **2007**, *664*, 862–878. [CrossRef]
115. Niikura, H.; Takada, M.; Yokoyama, S.; Sumi, T.; Masaki, S. Constraints on Earth-mass primordial black holes from OGLE 5-year microlensing events. *Phys. Rev. D* **2019**, *99*, 083503. [CrossRef]
116. Mróz, P.; Udalski, A.; Szymański, M.K.; Soszyński, I.; Pietrukowicz, P.; Kozłowski, S.; Poleski, R.; Skowron, J.; Ulaczyk, K.; Gromadzki, M.; et al. Limits on Planetary-mass Primordial Black Holes from the OGLE High-cadence Survey of the Magellanic Clouds. *Astrophys. J. Lett.* **2024**, *976*, L19. [CrossRef]
117. Calchi Novati, S. Pixel lensing: Microlensing towards M31. *Gen. Rel. Grav.* **2010**, *42*, 2101–2126. [CrossRef]
118. Calchi Novati, S.; Paulin-Henriksson, S.; An, J.; Baillon, P.; Belokurov, V.; Carr, B.J.; Crézé, M.; Evans, N.W.; Giraud-Héraud, Y.; Gould, A.; et al. POINT-AGAPE pixel lensing survey of M31: Evidence for a MACHO contribution to galactic halos. *Astron. Astrophys.* **2005**, *443*, 911. [CrossRef]
119. de Jong, J.T.A.; Widrow, L.M.; Cseresnjes, P.; Kuijken, K.; Crotts, A.P.S.; Bergier, A.; Baltz, E.A.; Gyuk, G.; Sackett, P.D.; Uglesich, R.R.; et al. MACHOs in M 31? Absence of evidence but not evidence of absence. *Astron. Astrophys.* **2006**, *446*, 855–875. [CrossRef]
120. Calchi Novati, S.; Bozza, V.; Bruni, I.; Dall'Ora, M.; De Paolis, F.; Dominik, M.; Gualandi, R.; Ingrosso, G.; Jetzer, P.; Mancini, L.; et al. The M31 Pixel Lensing PLAN Campaign: MACHO Lensing and Self-lensing Signals. *Astrophys. J.* **2014**, *783*, 86. [CrossRef]
121. Sugiyama, S.; Takada, M.; Yasuda, N.; Tominaga, N. Microlensing constraints on Primordial Black Hole abundance with Subaru Hyper Suprime-Cam observations of Andromeda. *arXiv* **2026**, arXiv:2602.05840. [CrossRef]
122. Smyth, N.; Profumo, S.; English, S.; Jeltema, T.; McKinnon, K.; Guhathakurta, P. Updated Constraints on Asteroid-Mass Primordial Black Holes as Dark Matter. *Phys. Rev. D* **2020**, *101*, 063005. [CrossRef]
123. Mróz, P.; Udalski, A. Eppur non si trovano Vol. 2: No Planetary-mass Primordial Black Holes toward the Andromeda Galaxy. *arXiv* **2026**, arXiv:2604.00111.
124. Griest, K.; Cieplak, A.M.; Lehner, M.J. Experimental Limits on Primordial Black Hole Dark Matter from the First 2 yr of Kepler Data. *Astrophys. J.* **2014**, *786*, 158. [CrossRef]
125. Kavanagh, B. PBHBounds. Available online: https://zenodo.org/records/3538999 (accessed on 19 April 2026).
126. Cieplak, A.M.; Griest, K. Improved Theoretical Predictions of Microlensing Rates for the Detection of Primordial Black Hole Dark Matter. *Astrophys. J.* **2013**, *767*, 145. [CrossRef]
127. DeRocco, W.; Frangipane, E.; Hamer, N.; Profumo, S.; Smyth, N. Revealing terrestrial-mass primordial black holes with the Nancy Grace Roman Space Telescope. *Phys. Rev. D* **2024**, *109*, 023013. [CrossRef]
128. Fardeen, J.; McGill, P.; Perkins, S.E.; Dawson, W.A.; Abrams, N.S.; Lu, J.R.; Ho, M.F.; Bird, S. Astrometric Microlensing by Primordial Black Holes with the Roman Space Telescope. *Astrophys. J.* **2024**, *965*, 138. [CrossRef]
129. Drlica-Wagner, A.; Mao, Y.Y.; Adhikari, S.; Armstrong, R.; Banerjee, A.; Banik, N.; Bechtol, K.; Bird, S.; Boddy, K.K.; Bonaca, A.; et al. Probing the Fundamental Nature of Dark Matter with the Large Synoptic Survey Telescope. *arXiv* **2019**, arXiv:1902.01055. [CrossRef]
130. Verma, H.; Rentala, V. Astrometric microlensing of primordial black holes with Gaia. *J. Cosmol. Astropart. Phys.* **2023**, *05*, 045. [CrossRef]
131. Bird, S.; Albert, A.; Dawson, W.; Ali-Haimoud, Y.; Coogan, A.; Drlica-Wagner, A.; Feng, Q.; Inman, D.; Inomata, K.; Kovetz, E.; et al. Snowmass2021 Cosmic Frontier White Paper: Primordial black hole dark matter. *Phys. Dark Univ.* **2023**, *41*, 101231. [CrossRef]
132. Pruett, K.; Dawson, W.; Medford, M.S.; Lu, J.R.; Lam, C.; Perkins, S.; McGill, P.; Golovich, N.; Chapline, G. Primordial Black Hole Dark Matter Simulations Using PopSyCLE. *Astrophys. J.* **2024**, *970*, 169. [CrossRef]
133. Crispim Romao, M.; Croon, D.; Crossey, B.; Godines, D. Dark classification matters: Searching for primordial black holes with LSST. *J. Cosmol. Astropart. Phys.* **2025**, *10*, 066. [CrossRef]


**Disclaimer/Publisher's Note:** The statements, opinions and data contained in all publications are solely those of the individual author(s) and contributor(s) and not of MDPI and/or the editor(s). MDPI and/or the editor(s) disclaim responsibility for any injury to people or property resulting from any ideas, methods, instructions or products referred to in the content.